

PRINCIPAL COMPONENT CLASSIFICATION

Rozenn Dahyot

Department of Computer Science, Maynooth University, Ireland

ABSTRACT

We propose to directly compute classification estimates by learning features encoded with their class scores. Our resulting model has an encoder-decoder structure suitable for supervised learning, it is computationally efficient and performs well for classification on several datasets.

Index Terms— Supervised Learning, PCA, classification

1. INTRODUCTION

The choice of data encoding for defining inputs and outputs of machine learning pipelines contributes substantially to their performance. For instance, adding positional encoding in the inputs has shown useful for Convolutional Neural Networks [1] and for Neural radiance Fields [2]. Here, we propose to add vectors of class scores as part of inputs to learn principal components suitable for predicting classification scores. Performance of our proposed frugal model is validated experimentally on datasets *wine*, *australian* [3, 4] and *MNIST* [5] for comparison with metric learning classification [6, 4, 7], and deep learning [5, 8].

2. PRINCIPAL COMPONENT CLASSIFICATION

In supervised learning, we consider available a dataset $\mathcal{B} = \{(\mathbf{x}^{(i)}, \mathbf{y}^{(i)})\}_{i=1, \dots, N}$ of N observations with $\mathbf{x} \in \mathbb{R}^{d_x}$ denoting the feature vector of dimension d_x and $\mathbf{y} \in \mathbb{R}^{n_c}$ the indicator class vector where n_c is the number of classes. All coordinates of $\mathbf{y}^{(i)}$ are equal to zero at the exception of its coordinate $y_j^{(i)}$ that is equal to 1 if $\mathbf{y}^{(i)}$ is indicating that feature vector $\mathbf{x}^{(i)}$ belongs to class $j \in \{1, \dots, n_c\}$.

Principal Component Analysis (PCA) [9] is a standard technique for dimension reduction often used in conjunction with classification techniques [6]. In PCA, the principal components correspond to the eigenvectors of the covariance matrix Σ ranked in descending order of their associated eigenvalues, where $\Sigma = \frac{1}{N} \mathbf{X} \mathbf{X}^T$ and $\mathbf{X} = [\mathbf{x}^{(1)}, \dots, \mathbf{x}^{(N)}]$. These principal components provide an orthonormal basis in the feature space. Retaining only the ones associated with the highest eigenvalues allow to project \mathbf{x} in a very small dimensional

eigenspace (data embedding). Such PCA based representation has been used for learning images of objects, to perform detection and registration [10, 11, 12], and has a probabilistic interpretation [13]. PCA for dimensionality reduction of the feature space ignores information from the class labels and we propose next a new data encoding suitable for learning principal components that can be used for classification.

2.1. Data encoding with Class

Class score vectors have recently been used as node attributes in a graph model for image segmentation [14]. We propose likewise to use that information explicitly by creating a training dataset noted $\mathcal{T}_\alpha = \{\mathbf{z}_\alpha^{(i)}\}_{i=1, \dots, N}$ from the dataset \mathcal{B} , where each instance $\mathbf{z}_\alpha^{(i)}$ concatenates the feature vector $\mathbf{x}^{(i)}$ with its class vector $\mathbf{y}^{(i)}$ as follow:

$$\mathbf{z}_\alpha = (1 - \alpha) \cdot \begin{pmatrix} \mathbf{x} \\ \mathbf{0}_y \end{pmatrix} + \alpha \cdot \begin{pmatrix} \mathbf{0}_x \\ \mathbf{y} \end{pmatrix} \quad (1)$$

where $\mathbf{0}_x$ and $\mathbf{0}_y$ are the null vectors of feature space \mathbb{R}^{d_x} and class space \mathbb{R}^{n_c} respectively. The scalar $0 \leq \alpha \leq 1$ is controlling the weight of the class vector w.r.t. the feature vector, and it is a hyper-parameter in this new framework. The training dataset \mathcal{T}_α is stored in a data matrix noted $Z_\alpha = [\mathbf{z}_\alpha^{(1)}, \dots, \mathbf{z}_\alpha^{(N)}]$. The matrix Z_α concatenates vertically the matrix \mathbf{X} and the matrix $\mathbf{Y} = [\mathbf{y}^{(1)}, \dots, \mathbf{y}^{(N)}]$ as follows:

$$Z_\alpha = \begin{bmatrix} (1 - \alpha) \cdot \mathbf{X} \\ \alpha \cdot \mathbf{Y} \end{bmatrix} \quad (2)$$

We note $d_z = d_x + n_c$ the dimension of vectors \mathbf{z}_α , and the matrix Z_α is of size $d_z \times N$.

2.2. Principal components

The $d_z \times d_z$ covariance matrix Σ_α is computed as follow:

$$\Sigma_\alpha = \frac{1}{N} Z_\alpha Z_\alpha^T = \mathbf{U}_\alpha \Lambda_\alpha \mathbf{U}_\alpha^T \quad (3)$$

In our experiments, we used Singular Value Decomposition (SVD) to compute the diagonal matrix Λ_α of eigenvalues $\{\lambda_i\}_{i=1, \dots, d_z}$ of Σ_α and with the corresponding eigenvectors stored as columns in the matrix $\mathbf{U}_\alpha = [\mathbf{u}_1, \dots, \mathbf{u}_{d_z}]$. For large training dataset ($N \gg 0$), more efficient algorithms

This work was funded by the SFI Research Centre ADAPT (13/RC/2106 P2), and is co-funded by the European Regional Development Fund.

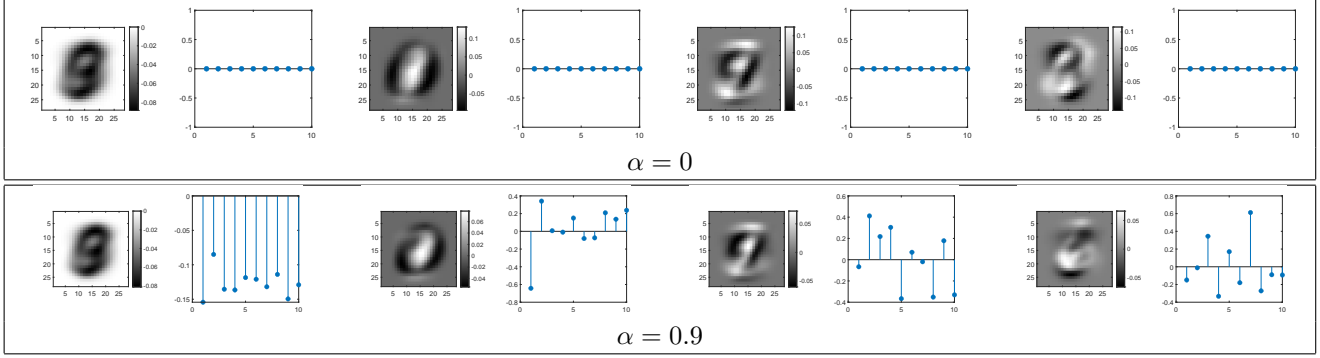


Fig. 1. Principal components for classification computed for Dataset MNIST. Effect of α on the first 4 principal components, \mathbf{u}_1 to \mathbf{u}_4 (left to right), computed for $\alpha = 0$ (top row) and $\alpha = 0.9$ (bottom row). For visualisation, eigenvector \mathbf{u} is shown as an image for the first d_x coordinates (in the feature \mathbf{x} -space) and as a plot for the remaining of its n_c components (in the class \mathbf{y} -space). Data is not centred (un-centred PCA) and the first component (left) captures the main deviation of the training dataset from the origin in the \mathbf{z} -space.

alternative to SVD can be used to compute the principal components [15]. Eigenvalues are sorted in decreasing order $\lambda_1 \geq \lambda_2 \geq \dots \geq \lambda_{d_z} \geq 0$ and their associated eigenvectors form an orthonormal basis of the \mathbf{z} -space. When $\alpha = 0$, only feature vectors appear in the vector \mathbf{z}_0 corresponding to the standard usage of PCA for dimensionality reduction of the feature space. When $\alpha > 0$, the principal components stored in U_α change away from the baseline U_0 (e.g. see Fig. 1).

2.3. Encoder & Decoder Model $\mathcal{M}_\alpha^{n_e}$

Dimensionality reduction is performed by only considering the first n_e eigenvectors associated with the n_e highest eigenvalues. Noting $U_\alpha^{n_e} = [\mathbf{u}_1, \dots, \mathbf{u}_{n_e}]$, the projection of any vector \mathbf{z} against the first n_e eigenvectors is computed as:

$$\mathbf{p}_\alpha^{n_e} = (U_\alpha^{n_e})^T \mathbf{z} \quad (4)$$

Projections of the training set \mathcal{T}_α can be visualised in the eigenspaces defined by a pair of principal components (cf. Fig. 2) providing renderings similar to TSNE [16].

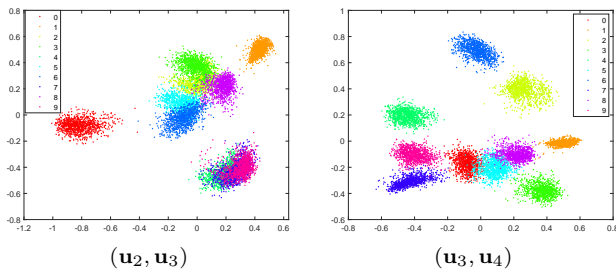


Fig. 2. Visualisation of projections. The training set $\mathcal{T}_{\alpha=0.9}$ is projected in the eigenspaces defined by pairs of our learnt principal components for dataset MNIST (shown Fig. 1).

Choosing a small number n_e of eigenvectors for projection allows to limit the number of computations, but it also needs to be large enough to capture useful information about

the dataset \mathcal{T}_α . The projection (Eq.4) is a linear encoder of \mathbf{z} which can be decoded as follows:

$$\hat{\mathbf{z}} = U_\alpha^{n_e} \mathbf{p}_\alpha^{n_e} = U_\alpha^{n_e} (U_\alpha^{n_e})^T \mathbf{z} \quad (5)$$

Our model $\mathcal{M}_\alpha^{n_e}$ is now explicitly defined (Eq. (5)) for transforming any input \mathbf{z} for transformation into an output $\hat{\mathbf{z}}$, using the learnt parameters (matrix $U_\alpha^{n_e}$) for the chosen hyper-parameters α and n_e (cf. Fig. 3). From the output $\hat{\mathbf{z}}$, the

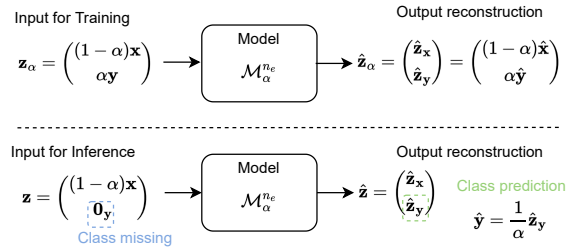


Fig. 3. Using model $\mathcal{M}_\alpha^{n_e}$: At training stage, hyper-parameters α and n_e are chosen, principal components $U_\alpha^{n_e}$ are computed as parameters for model $\mathcal{M}_\alpha^{n_e}$. Note that the reconstruction error $\mathbb{E}_{\mathcal{T}_\alpha} [\|\mathbf{z}_\alpha - \hat{\mathbf{z}}_\alpha\|]$ is minimized when using $U_\alpha^{n_e}$. At test time, the input used is proportional to \mathbf{z}_0 and a class prediction appears as part of the output reconstruction.

subvector $\hat{\mathbf{y}}$ is analysed such that the class $j \in \{1, \dots, n_c\}$ is identified by locating the highest valued coordinate of vector $\hat{\mathbf{y}}$:

$$\hat{j} = \arg \max_{j=1, \dots, n_c} \{\hat{\mathbf{y}}^T = [\hat{y}_1, \dots, \hat{y}_j, \dots, \hat{y}_{n_c}]\} \quad (6)$$

Estimates $\hat{\mathbf{y}}$ can also be visualised in the \mathbf{y} -space (cf. Fig. 4).

3. EXPERIMENTAL RESULTS

We rescale feature vectors \mathbf{x} so that the \mathbf{x} -space is an hyper-cube of volume 1. For MNIST dataset, all pixel values are scaled between 0 and 1 by dividing by 255. For the *wine*

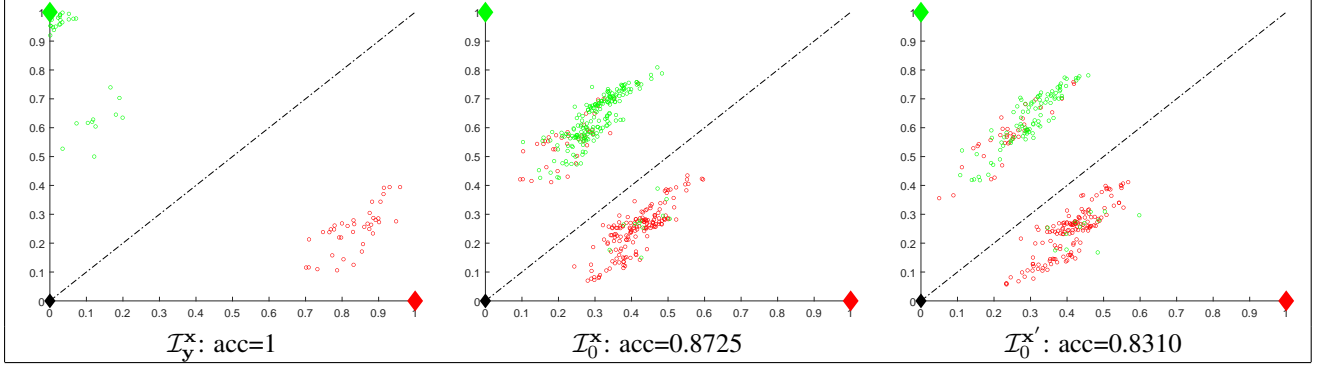


Fig. 4. Visualisation in the \mathbf{y} -space. Dataset *australian*: visualisation of the outputs $\hat{\mathbf{y}}$ (dots colour coded with the ground truth class label) in the class \mathbf{y} -space of dimension $n_c = 2$ computed with model $\mathcal{M}_{\alpha=0.5}^{n_e=4}$. The black diamond shows the class input to our model for sets \mathcal{I}_0^x and $\mathcal{I}_0^{x'}$; the red and green diamonds are the ideal class vectors used as part of the input in set \mathcal{I}_y^x (cf. Sec. 3).

and *australian* datasets, all feature dimensions are re-scaled to 1 by dividing by their corresponding maximum found in the dataset. For the *australian* dataset, we have used 200 instances per class for creating a balanced training set \mathcal{B} ($N = 2 \times 200 = 400$) and the remaining $N' = 290$ instances are used for the set \mathcal{B}' (a random allocation of instances is performed between \mathcal{B} and \mathcal{B}'). Likewise for the *wine* dataset, 40 instances per class are used for creating a balanced training set \mathcal{B} ($N = 3 \times 40 = 120$) and the rest $N' = 58$ is used for the test set \mathcal{B}' (random allocation is performed at every run). For the MNIST dataset, 1000 instances per class is used for training ($N = 10 \times 1000 = 10000$) and a balanced test set is likewise defined with $N' = 10 \times 1000 = 10000$ exemplars.

From the training set $\mathcal{B} = \{(\mathbf{x}^{(i)}, \mathbf{y}^{(i)})\}_{i=1, \dots, N}$, the set $\mathcal{T}_\alpha = \{\mathbf{z}_\alpha^{(i)}\}$ is used to compute the matrix of eigenvectors U_α . It is also used as a set of inputs noted $\mathcal{I}_y^x \equiv \mathcal{T}_\alpha$ for testing our model $\mathcal{M}_\alpha^{n_e}$: both feature vectors and class vectors are available as seen during training of the model $\mathcal{M}_\alpha^{n_e}$ therefore we expect accuracy reported for \mathcal{I}_y^x to be high if not perfect when the number n_e of eigenvectors is large enough to prevent any loss of information. In practice the class vector is not known and only the feature vector is available to be used as input of the our model $\mathcal{M}_\alpha^{n_e}$ (cf. Fig. 3). We propose to use the input \mathbf{z}_0 (multiply by $(1 - \alpha)$, cf. Eq. 1) that initialises all components in the class vector to 0s. From the training set $\mathcal{B} = \{(\mathbf{x}^{(i)}, \mathbf{y}^{(i)})\}_{i=1, \dots, N}$, we create a test set of inputs noted $\mathcal{I}_0^x = \{(1 - \alpha)\mathbf{z}_0^{(i)}\}$ that have the same feature vectors as seen during training by the model but without its class information. From \mathcal{B}' unseen for computing the matrix U_α , we create likewise a set of inputs noted $\mathcal{I}_0^{x'}$ to test our model for classification. For each set of inputs \mathcal{I}_y^x , \mathcal{I}_0^x and $\mathcal{I}_0^{x'}$, our model is used to estimate the class label (cf. Eq. 6) and we report the accuracy rate.

Figure 5 shows classification accuracies colour coded as heat maps computed for sets \mathcal{I}_y^x , \mathcal{I}_0^x and $\mathcal{I}_0^{x'}$, for a range of values $0 \leq \alpha \leq 1$ and $n_e \in \{1, 2, \dots, d_z\}$. In practice, the hyper-parameters n_e and α can be chosen with grid search on

these heat-maps computed with \mathcal{I}_0^x (acting as validation set) in order to get the best accuracy possible for the minimum number n_e of principal components that affect the computational cost of our model. As expected, results on set \mathcal{I}_y^x often reach perfect accuracy (Acc=1). The classification accuracy for sets \mathcal{I}_0^x and $\mathcal{I}_0^{x'}$ has a similar behaviour showing that our approach generalised well to unseen features.

For MNIST dataset, heat-maps look smooth on the hyper-parameter space and we see that increasing α allows to concentrate classification efficiency on the first 16 eigenvectors for \mathcal{I}_0^x and $\mathcal{I}_0^{x'}$ (cf. Fig. 5). The classification accuracy for \mathcal{I}_0^x and $\mathcal{I}_0^{x'}$ decreases when too many eigenvectors are used: our model approximates (and converge to) the identity function (when $n_e = d_z$, cf. Eq. (5)) and therefore the model output corresponds to its input which does not provide any class prediction for \mathcal{I}_0^x and $\mathcal{I}_0^{x'}$. However, when compressing information in the encoder (i.e. choosing $n_e \ll d_z$), a class prediction appears as part of the output. For fair benchmark comparison, our models $\mathcal{M}_{0.9}^{16}$ and $\mathcal{M}_{0.02}^{618}$ are retrained¹ on the full training set (no data augmentation), and classification accuracy is computed for the full provided test set (cf. Tab 1).

Model	Accuracy	# Trainable para.
Ours $\mathcal{M}_{0.9}^{16}$	0.8093	12704
Ours $\mathcal{M}_{0.02}^{618}$	0.8541	490692
Efficient-CapsNet [8]	0.99	161000
LeNet [5]	0.99	60000

Table 1. Benchmark on MNIST. Accuracy result reported for our models $\mathcal{M}_{0.9}^{16}$ and $\mathcal{M}_{0.02}^{618}$ (trained here on the $N = 60,000$ images) is computed using the full test set ($N' = 10,000$ test images). Its number of trainable parameters corresponds to the number of elements in matrix U_α^{2e} (i.e. $n_e \times d_z$). While not competing for accuracy with deep learning models, our results with our models took less than 2 seconds for each $\mathcal{M}_{0.9}^{16}$ and $\mathcal{M}_{0.02}^{618}$ to compute -both training and testing - in this experiment highlighting how frugal our model is.

¹Demo code available at <https://github.com/Roznn/DEC>

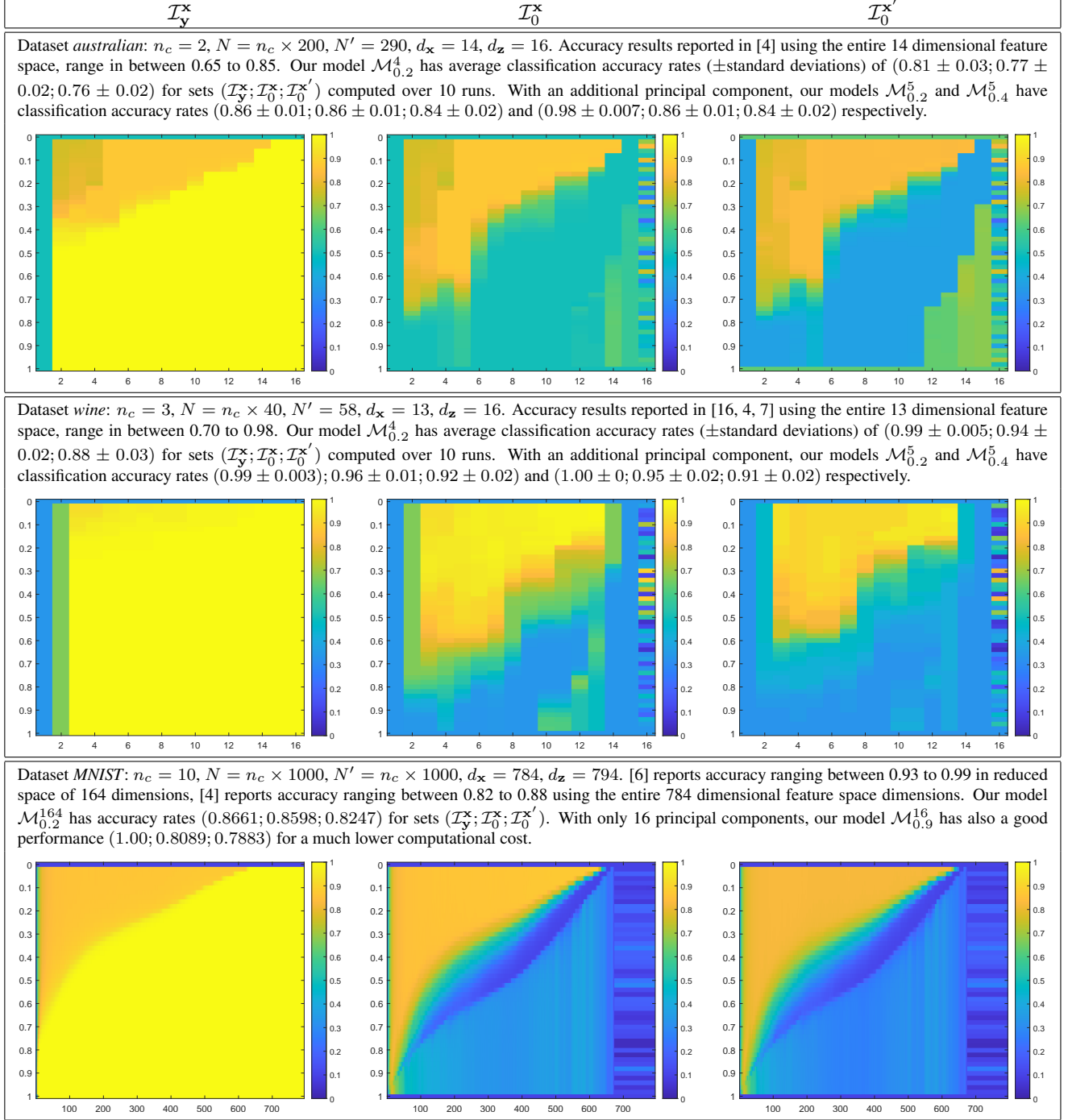


Fig. 5. Classification accuracy rate (colour coded) over the hyper-parameter space $n_e = [1 : 1 : d_z]$ (abscissa) and $\alpha = [0 : 0.02 : 1]$ (y-axis), with comparison to KNN classification results using metric learning [16, 4, 7].

4. CONCLUSION

We have introduced a new linear, PCA inspired, classifier that has encouraging accuracy, can learn from small training datasets as well as larger ones. It has very low computational complexity compared to deep learning models. Fu-

ture work will investigate combining multiple models learning from smaller image patches (as done in CNNs) to improve accuracy on image dataset (ensemble learning), and what alternative strategy to grid search could be used to select hyper-parameters.

5. REFERENCES

- [1] Rosanne Liu, Joel Lehman, Piero Molino, Felipe Petroski Such, Eric Frank, Alex Sergeev, and Jason Yosinski, “An intriguing failing of convolutional neural networks and the coordconv solution,” in *Advances in Neural Information Processing Systems*, S. Bengio, H. Wallach, H. Larochelle, K. Grauman, N. Cesa-Bianchi, and R. Garnett, Eds. 2018, vol. 31, Curran Associates, Inc.
- [2] Ben Mildenhall, Pratul P. Srinivasan, Matthew Tancik, Jonathan T. Barron, Ravi Ramamoorthi, and Ren Ng, “Nerf: Representing scenes as neural radiance fields for view synthesis,” *Commun. ACM*, vol. 65, no. 1, pp. 99–106, dec 2021.
- [3] Dheeru Dua and Casey Graff, “UCI machine learning repository,” 2017, <http://archive.ics.uci.edu/ml>.
- [4] Pourya Habib Zadeh, Reshad Hosseini, and Suvrit Sra, “Geometric mean metric learning,” in *Proceedings of the 33rd International Conference on International Conference on Machine Learning - Volume 48*. 2016, ICML’16, p. 2464–2471, JMLR.org.
- [5] Y. Lecun, L. Bottou, Y. Bengio, and P. Haffner, “Gradient-based learning applied to document recognition,” *Proceedings of the IEEE*, vol. 86, no. 11, pp. 2278–2324, 1998.
- [6] Kilian Q. Weinberger and Lawrence K. Saul, “Distance metric learning for large margin nearest neighbor classification,” *J. Mach. Learn. Res.*, vol. 10, pp. 207–244, jun 2009.
- [7] A. Collas, A. Breloy, G. Ginolhac, C. Ren, and J.-P. Ovarlez, “Robust geometric metric learning,” in *30th European Signal Processing Conference (EUSIPCO)*, Belgrade, Serbia, 2022.
- [8] V. Mazzia, F. Salvetti, and M. Chiaberge, “Efficient-capsnet: capsule network with self-attention routing,” *Scientific Reports*, vol. 11, no. 14634, 2021.
- [9] F. van der Heijden, R. P. W. Duin, D. de Ridder, and D. M.J. Tax, *Classification, Parameter Estimation and State estimation; An Engineering Approach using Matlab*, Wiley, 2004.
- [10] B. Moghaddam and A. Pentland, “Probabilistic visual learning for object representation,” *IEEE Transactions on Pattern Analysis and Machine Intelligence*, vol. 19, no. 7, pp. 696–710, 1997.
- [11] R. Dahyot, P. Charbonnier, and F. Heitz, “A bayesian approach to object detection using probabilistic appearance-based models,” *Pattern Analysis and Applications*, vol. 7, no. 3, pp. 317–332, Dec 2004.
- [12] C. Arellano and R. Dahyot, “Robust bayesian fitting of 3d morphable model,” in *Proceedings of the 10th European Conference on Visual Media Production*, New York, NY, USA, 2013, CVMP ’13, pp. 9:1–9:10, ACM, <http://doi.acm.org/10.1145/2534008.2534013>.
- [13] Michael E. Tipping and Christopher M. Bishop, “Probabilistic principal component analysis,” *Journal of the Royal Statistical Society. Series B (Statistical Methodology)*, vol. 61, no. 3, pp. 611–622, 1999.
- [14] J. Chopin, J.-B. Fasquel, H. Mouchere, R. Dahyot, and I. Bloch, “Improving semantic segmentation with graph-based structural knowledge,” in *ICPRAI International Conference on Pattern Recognition and Artificial Intelligence*, 2022.
- [15] Ian Gemp, Brian McWilliams, Claire Vernade, and Thore Graepel, “EigenGame: PCA as a nash equilibrium,” in *International Conference on Learning Representations*, 2021.
- [16] Laurens van der Maaten and Geoffrey Hinton, “Visualizing data using t-sne,” *Journal of Machine Learning Research*, vol. 9, no. 86, pp. 2579–2605, 2008.